JOURNAL OF MATERIALS SCIENCE 21 (1986) 3317–3332

Erosive wear of polymer surfaces by steel ball blasting

KLAUS FRIEDRICH
Polymer and Composites Group, Technical University of Hamburg–Harburg, 2100 Hamburg 90, West Germany

The erosion behaviour of a variety of polymeric materials has been studied using steel balls at 57 m sec^{-1} in an air-blast rig. It is shown that the softer polymers (polyethylene, polypropylene, polybutene-1) exhibit an incubation period prior to stabilizing to a linear erosion rate, here defined as reduction in thickness per testing time. The more brittle polymer, polystyrene, on the other hand, shows no incubation time and possesses the highest erosion rate. Further effects can arise from the morphology of semicrystalline polymers. In particular, it was found that a coarse spherulitic microstructure in polypropylene wears much faster than a fine spherulitic one. A decrease in testing temperature generally increases the wear rate. The individual mechanisms of erosive wear are illustrated by SEM micrographs of the worn surfaces. It is suggested that a "brittleness index" of the form (hardness H/fracture energy G_{Ic}) is a good indicator for the erosion resistance of polymeric materials.

1. Introduction

If solid particles impinge against a target surface and cause local damage combined with material removal, this kind of wear is generally referred to as erosion [1, 2]. The mechanisms of material removal involved in the wear process are determined by the intensity of surface damaging due to repetitive impact events and/or severe scratching of the target material. For example, scratching of ceramic surfaces produces either brittle scratches with chip formation by multiple cracking or ductile scratches with plastic deformation and final rupture or cutting [3]. Surface fatigue and the formation of a residual tensile stress field during repeated impacting of metals have been found to be responsible for the initiation of microcracks in subsurface layers and the subsequent flaking and detachment of wear particles [4, 5]. All of these mechanisms are not restricted to ceramic or metallic target materials but may take place under erosion of polymer surfaces as well. Their cumulative occurence depends, however, on the type of polymer tested (molecular structure, morphology, structure–property profile), and on the testing conditions, in particular the testing temperature, impact angle, type of erodent etc. Thus, as for other materials and other wear situations, erosive wear resistances is not a material property but depends strongly on the system in which surfaces function [6]. Schematically this is illustrated in Fig. 1.

The effects of various testing parameters on the erosive wear behaviour of different kinds of polymer have been demonstrated by several authors in the past. A brief review on this subject was performed quite recently by Walley *et al.* [7]. Many of the ductile polymers possess an angular dependence of erosion which is similar to that for ductile metals, peaking at around 30° [8–10]. More brittle materials, on the other hand, may exhibit their highest erosive wear rates at an impact angle of 90° [2, 11]. Tilly and Sage [12] showed that various brittle ductile polymers undergo the same velocity dependence of erosion as metals, namely a power law of $v^{2.3}$. With respect to the size and type of the erodent material, two trends can be considered to be valid for harder and/or more brittle materials such as metals, ceramics or epoxies: the erosive wear increases the higher the hardness of the erodent and the larger the erosive particle size (until a level of saturation is reached in both cases) [2, 9, 11, 12]. In ductile polymers, however, the situation may be quite different: (i) due to their relatively low hardness no pronounced effects of changes in the hardness of the usually much harder erodent materials should be expected [9], and (ii) it has been observed that size effects of the erosive particles only play a major role in a diameter range under about 100 μm [12].

Studies on the erosion resistance of different polymer target materials have been reported in several papers (e.g. [12–17]). Under certain testing conditions, different polymers may exhibit a range of erosion rates spanning more than two orders of magnitude [13, 14]. This must be considered as a clear indication that the wear properties are highly dependent on the molecular structure [18] and the polymer morphology. For erosive wear tests carried out at room temperature (RT), the following trends of erosion rate as a function of polymer structure can be assumed:

(a) erosion is higher for polymers with a glass transition temperature T_g above RT relative to those with T_g < RT;

(b) for T_g < RT, the wear rate decreases the greater the difference between the experimental temperature and T_g [19];

0022–2461/86 $03.00 + .12

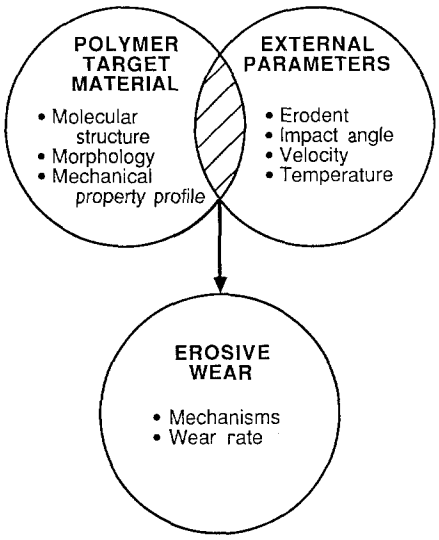

Figure 1 Material properties and testing parameters which may influence the erosive wear results.

(c) erosion is least for low-modulus, highly elastic rubbers or elastomeric polyurethanes;

(d) amorphous polymers usually erode faster than semicrystalline thermoplastics.

In addition, Tilly and Sage [12] illustrated that fibre reinforcement can help to reduce the erosive wear rate of brittle polymer matrices (such as epoxy (EP)), whereas the opposite may occur in the case of a ductile polymer matrix (such as polyamide (PA)). These results are in agreement with those found under sliding, abrasive wear conditions of different kinds of fibre-reinforced plastics [20, 21].

Walley *et al.* [7] pointed out that a connection with measurable mechanical properties, as demonstrated successfully by Ratner *et al.* [22] and Lancaster [23] for single-pass abrasion of different polymers, is not easy to transfer to erosion. This is mainly due to the very complex stress state within the target material under erosive impact conditions, the very high strain rates, and possible fatigue mechanisms [24]. Especially it was never found that the erosive wear rate is inversely proportional to the hardness. Although this relationship holds quite well for the erosive wear of metals [1, 8, 9] (but only in a lower hardness range [2]), for polymers exactly the opposite trend may take place. Analysing the test results presented by Brauer and Kriegel [14] many years ago in this respect gives clear evidence for different tendencies. This does not, however, mean that the hardness is the mechanical property of polymers which controls their erosive wear behaviour. A lower hardness is here only an indication that a greater amount of the impact energy of the erosive particles can be absorbed by elastic deformation of the target surface. Thus a lower amount of the impact energy is available for other mechanisms such as plastic deformation, crack initiation and local fracture.

To prevent the latter mechanisms leading to the production of wear debris, material properties other than hardness are of importance, for instance a high stress yield σ_y and (after σ_y is exceeded) a high strain to failure ε_f. This combination means that the material must possess a high fracture energy, or in general a high resistance against crack initiation and propagation under very complex (fatigue and/or impact) loading conditions. In fact, studies on severe rain erosion of different types of polymer have shown that within the typical scatter of these data some kind of a relationship between the erosive wear resistance and the notched impact fracture energy exists [13, 18].

Although hardness and impact fracture energy of polymeric materials can be separately considered to give a rough indication of their erosive wear behaviour, it probably makes more sense to build up a comparative figure involving both these parameters. Lamy [3] has suggested using the quantity H/K_c (H = hardness, K_c = static fracture toughness) as a convenient "brittleness index" for materials subjected to surface scratching in abrasive or erosive processes. He found for the wear rate of materials of different fracture energy classes an increase with increasing "brittleness index". A modified correlation of the form $H^{0.5}/K_c^2$ has been found to work quite well in describing the erosion resistance of brittle target materials [25]. In the present approach an attempt is made to use a similar relationship for the description of the erosive wear behaviour of different thermoplastic polymers. An additional objective is to elucidate the typical wear mechanisms which may occur as a result of differences in molecular structure, mobility and polymer morphology.

2. Experimental details

2.1. Target materials

The target materials used in the present investigation provided a reasonably wide range of mechanical behaviour and microstructure for study. Commercially available materials (Table I) were obtained from the manufacturers (PS, PE and PP from BASF, Ludwigshafen, West Germany; PB–1 from CWH, Marl-Hüls, West Germany) as compression-moulded rectangular plaques, 20 mm in thickness. The material selection was done in such a way that one polymer had a glass transition temperature T_g far above RT (PS, $T_g \approx 90°$ C), and one polymer with T_g far below RT (PE, $T_g \approx -80°$ C). The T_g values of the other polymers covered the intermediate range between the T_g of PE and RT: PB-1 with $T_g \simeq -35°$ C and PP with $T_g \approx 0°$ C [26]. In order to get an idea about the mechanical characteristics of the different polymers as a function of temperature, all of them were tested with respect to their notch impact energy (German Standard DIN 53453) and their ball indentation hardness

TABLE I Commercial polymers tested

Material	Code	Morphology	Company type
Polystyrene	PS	Amorphous	168N
Polyethylene	PE	Semicrystalline	6011L
Polypropylene	PP-A	Semicrystalline 5% atactic	1120LX
Polypropylene	PP-B	Semicrystalline 20% atactic	1320L
Polybutene-1	PB-1	Semicrystalline	–

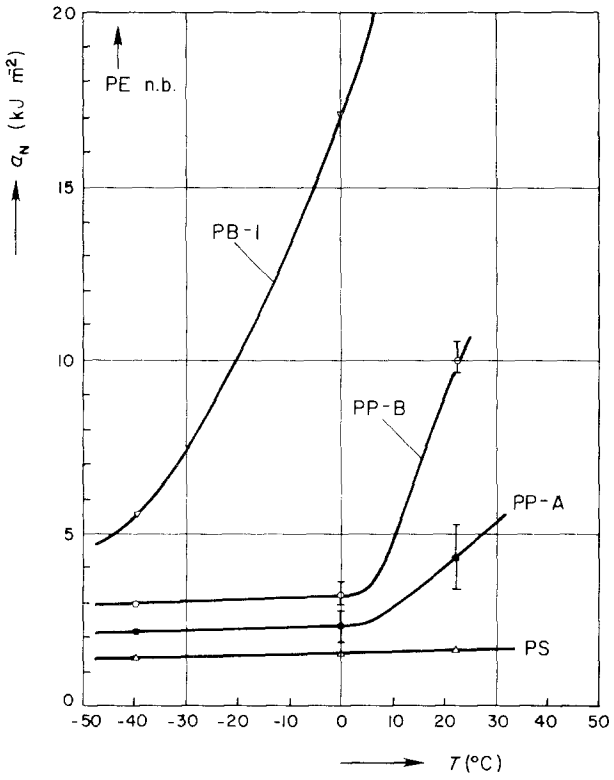

Figure 2 Notch impact energy, a_N, against testing temperature, T, for the commercial materials used in this study.

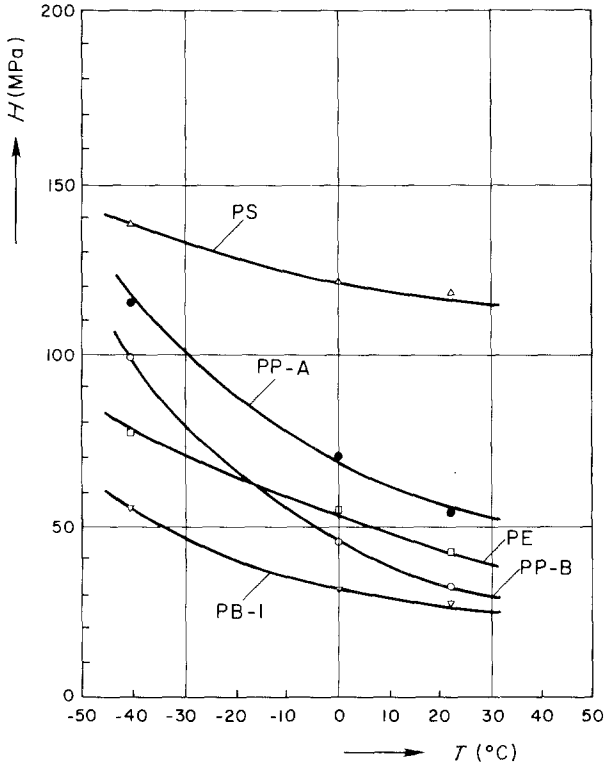

Figure 3 Ball indentation hardness of the polymers of this study as a function of testing temperature.

(German Standard DIN 56456). The results are represented in Figs 2 and 3 over a temperature range from $-40°$ C to RT (23° C). The differences in T_g are clearly reflected in the data for the notch impact energy. They indicate a high brittleness of PS over the whole temperature range tested, a brittle–ductile transition of PP-A and PP-B above $T = 0°$ C, and an enormous increase in toughness of PB-1 within the range -40 to 0° C. No impact fractures could be obtained for PE at all, nor for PB-1 at RT. The hardness of all the polymers increased with decreasing temperature (Fig. 3), but the most pronounced effect was found for the two kinds of PP when passing their T_g.

Concerning the PP samples, several modifications were used in this study:

(a) PP-A with a morphology as received after compression-moulding by the manufacturer (fine spherulitic, spherulite diameter $\bar{D}_s \simeq 20\,\mu$m, degree of crystallinity $X_c \simeq 55\%$),

(b) PP-B with similar spherulite size, but a lower degree of crystallinity ($X_c \simeq 45\%$) as a result of its higher atactic content.

In addition, two different PP-A morphologies (PP-A-I and PP-A-II) were produced in the laboratory in order to study the effects of microstructure on the erosion of a given polymeric material (Table II). Details of typical thermal treatments to obtain different morphologies in PP are described in previous papers [27–29]. Examples of the morphologies of PP-A-I and PP-A-II are shown in Fig. 4.

TABLE II Thermal treatment and morphology of polypropylene samples

Material	Thermal treatment	Morphology
Polypropylene PP-A-I	Melt-quenched and annealed	Fine spherulitic, high crystallinity
Polypropylene PP-A-II	Isothermally crystallized from melt	Coarse spherulitic, high crystallinity

2.2. Testing procedure

The particles used for the erosion measurements were steel balls, type "cutwire", with a diameter of $\bar{D} \simeq 500\,\mu$m (Fig. 5). They were poured into an apparatus designed to feed the erosive particles into a high-velocity air stream which propelled the particles against the specimen surface (Fig. 6). Under a constant air pressure of $p = 1.75$ bar (175 kPa) (controlled by a reduction valve) the particles were accelerated by passing them through a nozzle. In this way, a particle mass flow of $\dot{M} = \Delta M/\Delta t = 4.6\,\mathrm{g\,sec^{-1}}$ was achieved. The distance between the tip of the nozzle and the specimen surface was 25 mm, and the velocity of the particles at the moment of impact could be calculated as $v = 57\,\mathrm{m\,sec^{-1}}$. The corresponding impact energy each particle carried at the time of contact with the target was around $W^0 \approx 10^{-3}$ J.

Fig. 7a illustrates the specimen geometry used in this study. The samples were mounted in a specimen holder which was arranged in such a way that the round, polished surface of the samples was normal to the stream of erosive particles. As the holder could be cooled by the use of different kinds of cooling liquid, it was possible to control the temperature of the specimen at a distance 3 mm away from the target surface. The two testing temperatures chosen for this investigation were $T_1 =$ RT; $T_2 = -35°$ C.

Measurements of the erosive wear as a function of

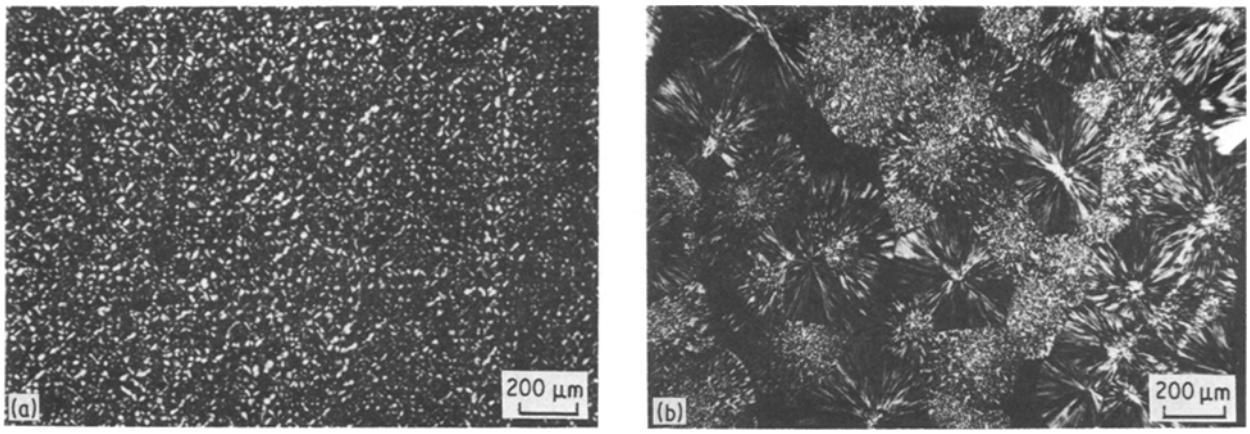

Figure 4 Transmitted optical light micrographs of thin sections taken from (a) the fine spherulitic morphology of PP-A-I, and (b) the coarse spherulitic morphology of PP-A-II.

testing time, Δt, were performed in two different ways:

(a) determining the mass loss, Δm, of the target to at least 1% accuracy by the use of an analytical balance,

(b) measuring the reduction in height, Δs (accuracy 1 μm) at the centre-line position of the rod-shaped specimens (Fig. 7b).

For several reasons which will be explained later, the latter quantity was used for the final calculation of the erosive wear rate, $\dot{E}_s$:

$$\dot{E}_s = \Delta s/\Delta t \quad (\mu\text{m sec}^{-1}) \tag{1}$$

A conversion into wear depth per mass of erodent can be easily done by multiplying Δt by $\dot{M}$. Using the maximum diameter of the impact crater ($\approx 65\%$ of the specimen diameter) a volumetric wear rate can be roughly calculated as

$$\dot{E}_v = \frac{\Delta s A_i}{\Delta t} \quad (\text{mm}^3\,\text{sec}^{-1}) \tag{2}$$

where A_i corresponds to the part of the specimen surface impacted by the erosive particles.

3. Results

3.1. Erosive wear data

Fig. 8 represents the reduction in specimen height of the five commercial polymers as a function of testing time. Two distinctively different trends in the erosion characteristic can be recognized:

(a) the hardest and most brittle polymer, the amorphous PS, having a T_g larger than the testing temperature (RT), shows almost right from the beginning a linear reduction in specimen length with time of erosion;

(b) the semicrystalline polymers (PE, PP, PB-1) with $T_g <$ RT exhibited S-shaped curves of Δs against t. Curves of similar shape have been found in the past for the erosive wear of Pyrex glass by glass beads [30] and for the rain erosion of different polymeric materials [13]. After an incubation period, a steady-state wear condition was achieved in which the wear rate was much lower than that found for PS.

Within the group of semicrystalline thermoplastics, PE was worn faster than the two kinds of PP or PB-1, in spite of its having the highest notch impact energy. The lowest erosion rate was measured for the highly atactic PP-B. The latter is compared with the other extreme, amorphous PS, in a single-logarithmic scale in Fig. 9, illustrating a difference in wear rate of almost two orders of magnitude.

Two characteristic differences in the wear behaviour can also be distinguished very easily when plotting the

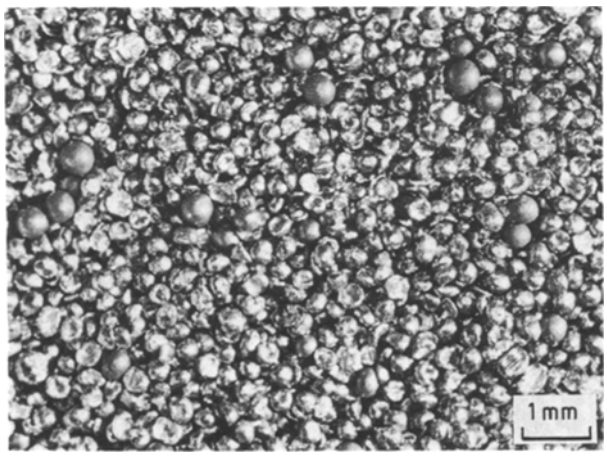

Figure 5 Photograph showing the size distribution and typical shapes of the steel balls used as the erodent in this study.

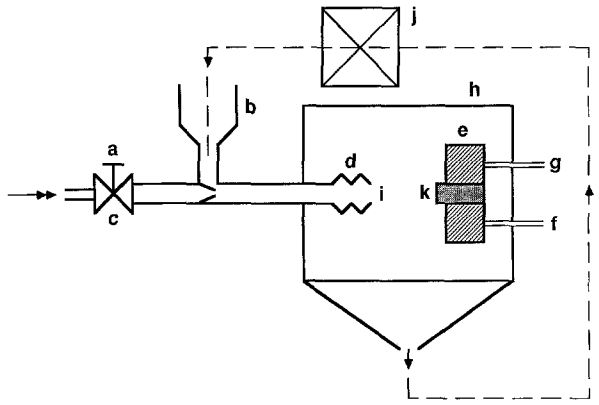

Figure 6 Schematic diagram of the air blast erosion rig: (a) valve, (b) abrasive feed and supply, (c) mixing nozzle, (d) nozzle thread, (e) specimen holder, (f) thermocouple, (g) entrance for cooling liquid, (h) test chamber, (i) nozzle, (j) erodent cleaning device, (k) specimen (double arrow = air stream, single arrows and dashed line = cyclic path of erosive particles).

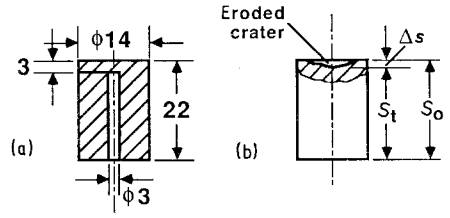

Figure 7 (a) Erosive wear specimen configuration (dimensions in mm), (b) location of height-reduction measurements in the eroded crater.

mass loss, Δm, against the testing time (Fig. 10). In the case of the semicrystalline materials, the shape of the curve is, however, different from the Δs against t plots. In agreement with results reported by Tilly and Sage [12] several years ago, the softer plastics exhibited very pronounced incubation times during which erodent material was obviously deposited on the target surfaces, thus producing a mass gain. In PE and the rigid PP-A, the situation stabilized within a relatively short period time in which the surface became saturated. Material removal due to erosion then exceeded deposition and a linear rate of mass loss was established. For the softer plastics PP-B and PB-1, however, no mass loss could be observed within the testing period chosen.

The effects of differences in polymer morphology on the erosive wear rate are illustrated in Fig. 11. PP-A-I with a fine spherulitic morphology and a higher crystallinity due to annealing at elevated temperatures exhibited a lower wear rate then the commercially available starter product PP-A. If, however, the microstructure is very coarse spherulitic, as in the case of PP-A-II, the erosion rate is much higher, and the extent of the incubation period is almost zero.

The influence of two different testing temperatures

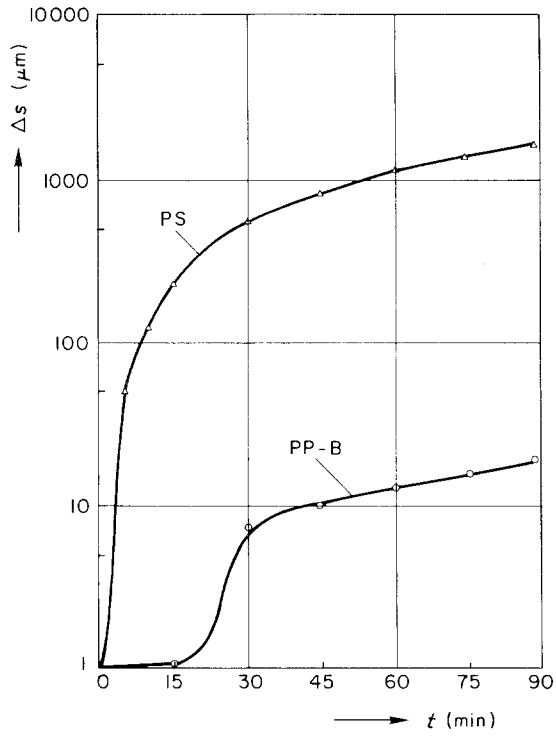

Figure 9 Logarithm of height reduction, Δs, against testing time for the polymers with lowest (PP-B) and highest (PS) erosion rate.

on the amount of damage due to erosion (expressed in terms of height reduction after 45 min) is illustrated on Figs 12a and b. Relative to the results obtained at RT, higher wear rates were expected if the specimens were cooled down to $-35°$ C. This particular temperature was chosen because it is below the T_g of PP, almost equal to the T_g of PB-1, and still above the T_g of PE. It turned out, however, that PE, PB-1 and PS did not show very pronounced increases in the erosion rate with decreasing temperature. Only in the PP

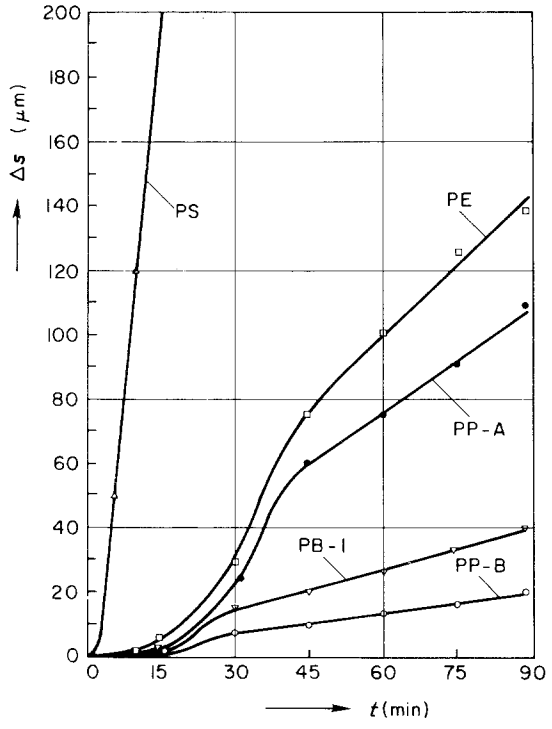

Figure 8 Reduction in specimen height, Δs, as a function of erosion time, t, for the commercial polymers at room temperature.

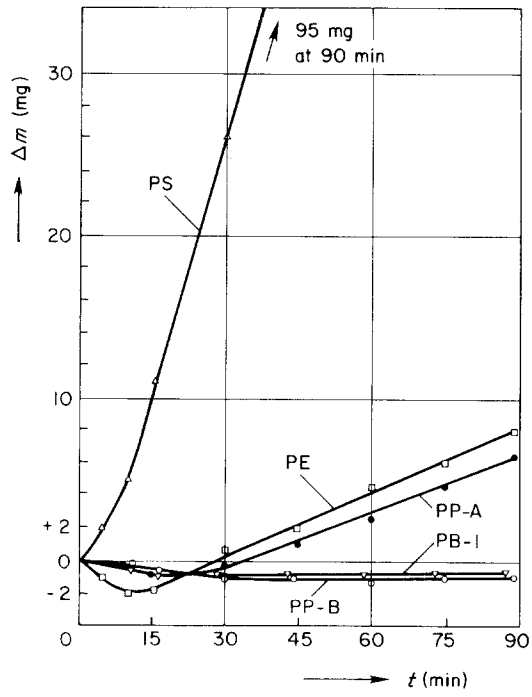

Figure 10 Corresponding diagram to Fig. 8, showing the change in specimen mass of the commercial polymers as a function of testing time.

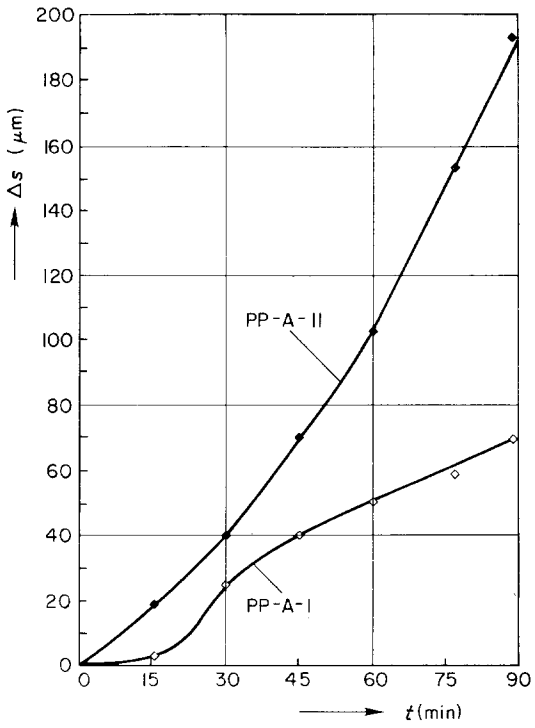

Figure 11 As Fig. 8, for two different PP morphologies.

modifications (PP-A, PP-B, PP-A-I, PP-A-II), which all undergo a ductile–brittle transition in the temperature range between RT and −35° C, were some clearer increases in wear rate detectable. It should be mentioned, though, that the temperatures given here do not represent the real temperatures in the contact region during erosion, because they were measured 3 mm away from the target surface.

3.2. Microscopy of erosive wear mechanisms

In the early stage of the erosion process, two extremely different types of wear behaviour are found as a result of different material characteristics. The brittle PS starts to wear almost immediately, and a typical erosion crater is formed very soon (Fig. 13a). The more ductile polymers such as PP-B or PB-1 show, however, a pronounced incubation period before material is really removed from the surface. Fig. 13b illustrates that during the incubation period of the ductile polymer, energy is dissipated in roughening the target surface. The roughening process includes a high degree of plastic deformation of the polymer under compressive and tensile stresses, mainly resulting in little surface bumps of material being pushed away from the individual impact locations. As the intensity of the particle stream is highest in the middle, this pushing away of material occurs more there than at other positions, so that after a while a reduction in specimen thickness can be found even though no mass loss may yet be detected. This will, however, take place as soon as deformed surface material is finally ruptured and removed with the particle stream, leading finally to the formation of a similar erosion crater to that seen for PS right from the beginning.

A cross-section through such a crater is schematically illustrated in Fig. 14a. Especially for PS it could be observed that the crater has a plateau-like profile, and that larger material chunks are preferentially broken off at the plateau edges (Fig. 14b). This does not exclude, however, that material removal occurs also on the plateaus themselves. Figs 15a to d show some typical examples of the formation of material chips on the plateau regions in PS, PP-A and PB-1. For the latter material it is shown, in addition, that no pronounced differences in the wear mechanisms exist at the two different temperature levels chosen (Figs 15c and d). In both cases, plastic deformation of the material around local impact events occurs, along with the formation of surface cracks in the vicinity. These microcracks are sometimes found to build up a dense network and seem to be caused by residual tensile stresses in the surface after repeatedly being impacted (Figs 16a to d). Again, it can be noted that there is no clear effect of the testing temperature on this particular surface damage mechanism.

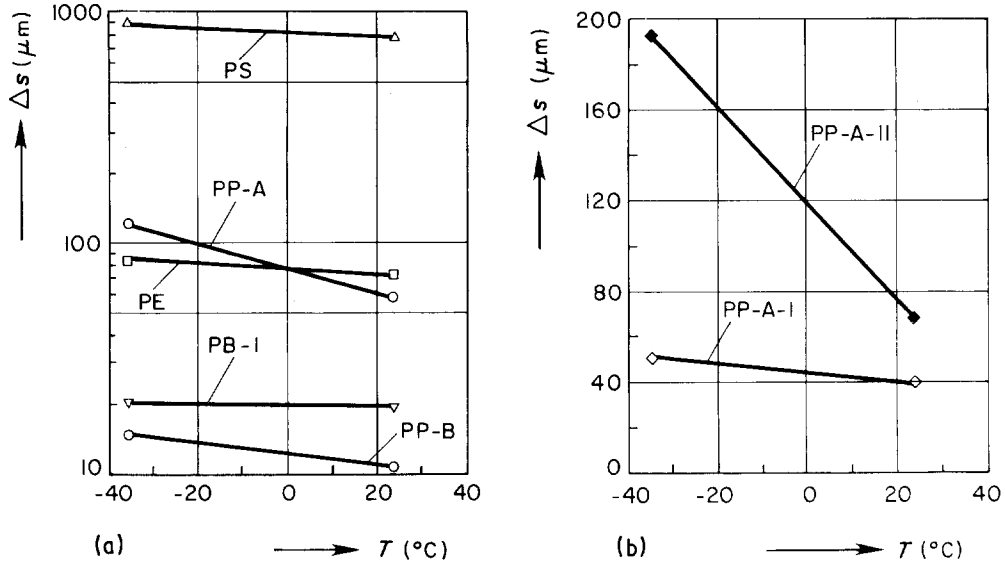

Figure 12 Effect of testing temperature on the reduction in specimen height Δs after 45 min of erosion: (a) commercial polymers (in logarithmic scale), (b) PP-morphologies (linear scale).

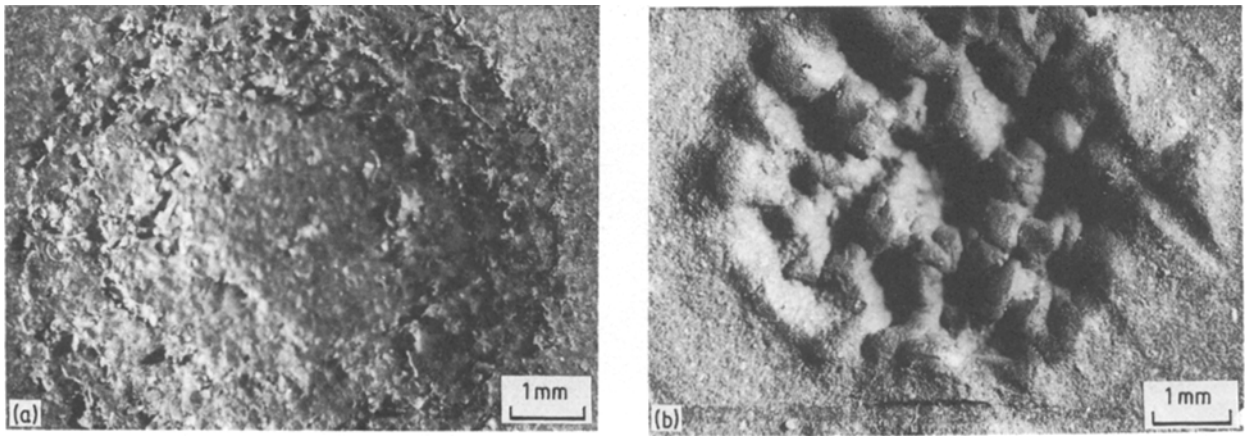

Figure 13 A 90° view on two specimen surfaces showing early stages of erosion (after 10 min) and the differences in wear behaviour as a result of different material properties: (a) in the brittle PS an erosion crater is formed right from the beginning, (b) highly plastically deformed surface of PB-1, typical for the incubation period of ductile polymers.

The latter statement is also valid for the embedding of foreign particles in the surface of the softer polymers. Figs 17a and b give two examples of erodent material deposited on the target surface of PE at $T = -35°$ C and PB-1 at RT, respectively. In all of these cases, the particles deposited on the surface were found to be much smaller than the regular size of the steel balls, indicating that besides the steel balls the erodent material contained broken, irregular-shaped steel particles and other impurities. The latter, including some dust or dirty layers on the steel balls, also appear as black spots on micrographs taken from thin sections of the erosive crater profiles of the softer polymers (Figs 18a to d). The profile sections indicate that a very high degree of plastic deformation has taken place in a narrow surface range. As a result, local cracks are initiated between highly torn polymer tips or bundles, which after rupture leads to the formation of flake-like wear debris.

Finally, Fig. 19 represents a mechanism of wear debris formation which only occurred on the surface of the coarse spherulitic PP-A-II samples. This kind of morphology is known to consist of highly crystalline, hard spherulites which are interconnected by very weak spherulite boundaries [27–29]. As cracking and fracture along these boundaries can happen very easily, these sites are also preferred locations for erosion damage (Figs 19a and b). In fact, a lot of zones were found on the eroded target of this material in which whole spherulites had been completely blasted out of the surface (Figs 19c and d).

4. Discussion

4.1. Model of the erosive wear process

Fig. 20 presents schematic plots of the height loss and mass loss as a function of time, typical for polymers with medium ductility. Within the incubation period, t_I, no height loss is detectable; at the same time, the mass of the target increases due to the deposition of erodent material on the target surface. The actual magnitude of the incubation time is dependent on the brittleness of the material investigated, decreasing with increasing brittleness. In the given study, the more brittle materials (PS, PP-A-II) exhibited no incubation period, whereas in the ductile systems measurable reductions in specimen height could first be detected after 10 to 15 min blasting time ($t_{I_{PE}} = t_{I_{PP\text{-}A\text{-}I}} = 10$ min; $t_{I_{PP\text{-}A}} = t_{I_{PP\text{-}B}} = t_{I_{PB\text{-}1}} = 15$ min).

The incubation phase is followed by a period of material removal which is reflected in a reduction of specimen height. Nevertheless it can happen that at the same time there is still enough erodent material deposited on the target surface, so that the measurable mass loss remains negative for a certain time (Δt_m). From the results of this study it can be concluded that Δt_m is especially long when the target surfaces are rather soft ($\Delta t_m > 90$ min for PB-1 and PP-B; $\Delta t_{m_{PP\text{-}A\text{-}I}} = 5$ min; $\Delta t_{m_{PE}} = 17$ min; $\Delta t_{m_{PP\text{-}A}} = 18$ min).

From a practical point of view it seems reasonable therefore to identify the slope of the Δs against t curve in the range where a steady-state condition is reached as the erosive wear rate of the material (according to Equation 1). Consider for example a pipeline which is

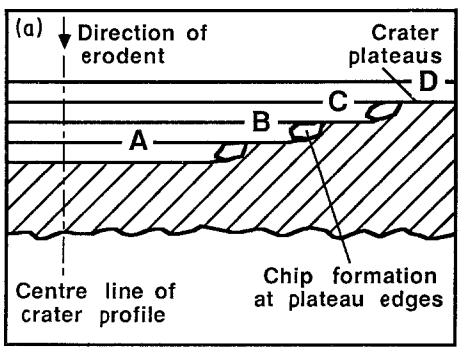

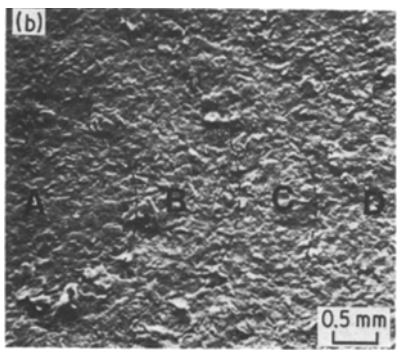

Figure 14 (a) Schematic sketch of a crater profile, and (b) SEM view into a crater of PS showing concentric regions where material had been removed on different plateau levels.

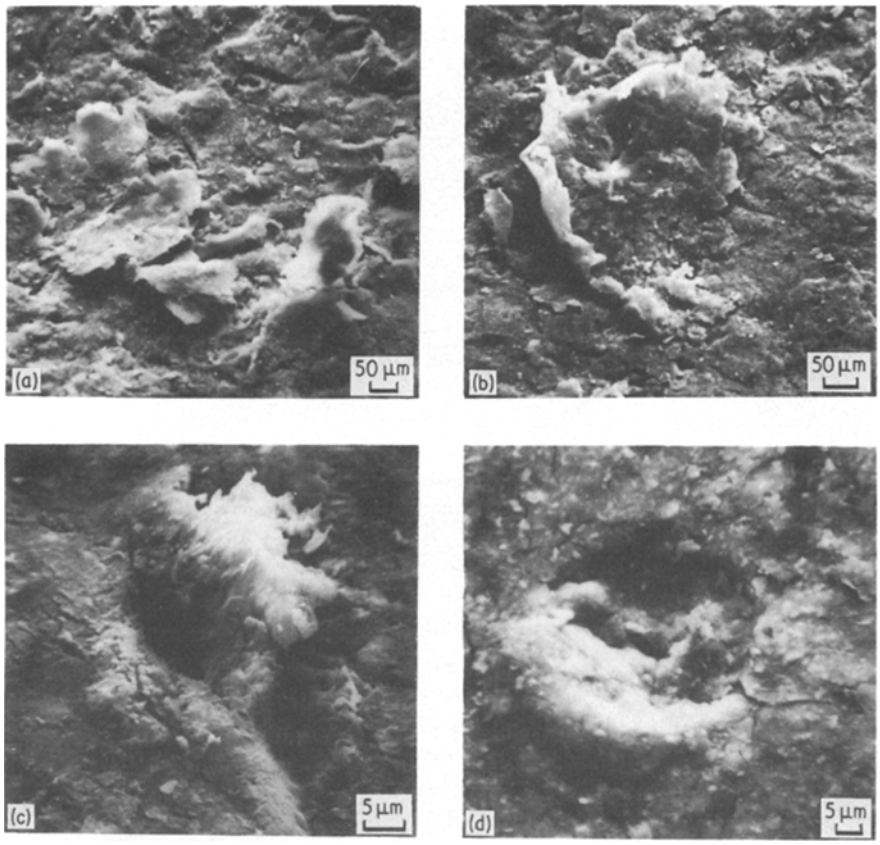

Figure 15 SEM micrographs showing events of local chip formation on the crater plateaus of (a) PS and (b) PP-A at room temperature. Micrographs (c) and (d) represent early stages in the formation of plastically deformed material regions on the surface of PB-1 at (c) room temperature and (d) $T = +35°$ C.

made of one of the very soft polymers and which transports particles capable of causing erosion of the pipeline wall. Leak failure of the part would occur when the thickness of the wall was reduced to zero. According to the results of this study, the latter can happen even if no reduction in mass of the polymer has taken place, simply by pushing plastically deformed polymer material away from the point of erosion. In practice, of course, thickness reduction due to local plastic deformation, deposition of erodent on the polymer surface and material removal from the surface due to cracking and rupture will occur simultaneously.

With respect to the erosion process as a result of 90°

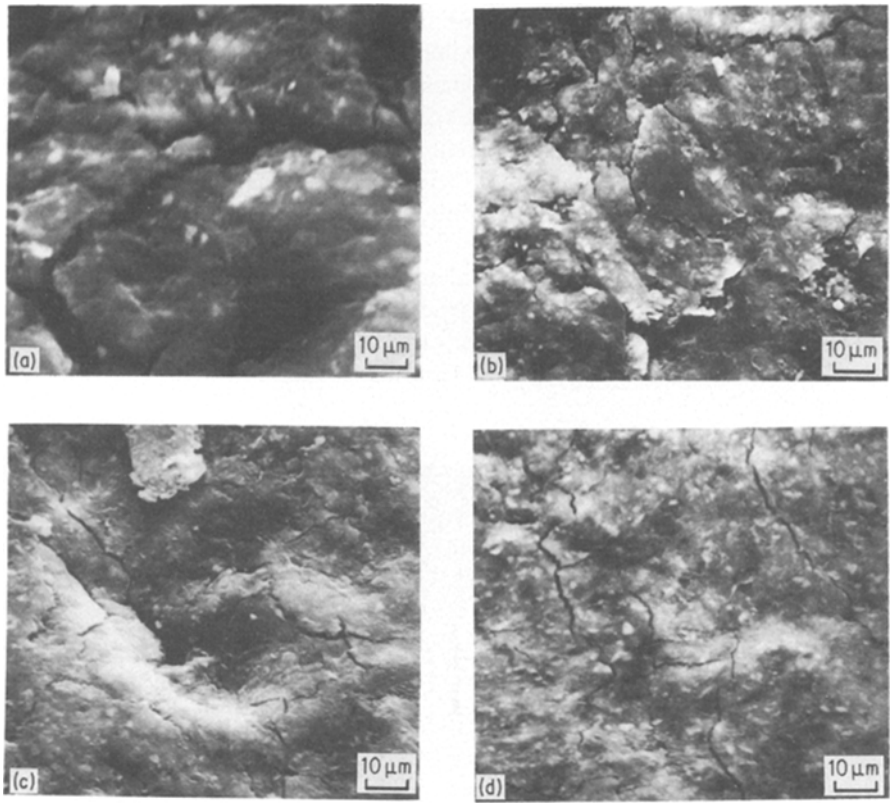

Figure 16 Typical networks of microcracks on the eroded surfaces of (a) PS at RT, (b) PP-A at RT, (c) PP-A-I at $-35°$ C and (d) PB-1 at $-35°$ C.

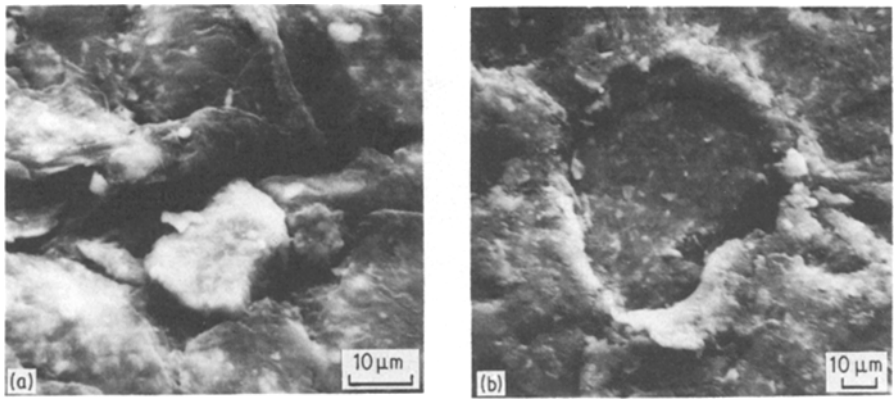

Figure 17 Sites of embedded foreign particles on the eroded surfaces of (a) PE at −35° C and (b) PB-1 at RT.

degree impacts by hard* steel balls on a relatively soft polymer target surface, one can distinguish between typical mechanisms associated with the different characters of the materials and their microstructure (Fig. 21). As a consequence of the repeated impact situation combined with a multiple loading and unloading of the target surface, the material is subjected to complicated cyclic stress fields, varying between tension and compression from point to point, and from one moment to another. In simplified form, this is illustrated by Diagram 2 in Fig. 21, although the actual situation is much more complicated [31, 32]. Fig. 21a represents the possible sequence of surface damaging as a result of repeated impact on a hard and brittle polymer. Damage is dominated by the formation of microcracks being initiated at the surface or in subsurface regions, which finally can coalesce to form brittle wear debris.

On the surface of softer and more ductile polymers, on the other hand, a high degree of plastic deformation takes place (Fig. 21b). In addition, crazes, shear bands, or cracks may be initiated within these regions. At the same time it is possible that smaller foreign particles are embedded in the deformed surface layer. Material removal occurs also here after the final combination of neighbouring cracks around deformed material tips, but the average time for this process is much longer due to the higher fracture energy (associated with better resistance against fatigue crack propagation) of this kind of polymer. The differences in mechanisms relative to the harder, brittle polymers are reflected in longer incubation periods t_I, in the mass gain period Δt_m, and in lower erosion rates $\dot{E}_s$.

A special situation arises in the case of the coarse spherulitic PP-A-II samples, in which the very soft spherulite boundaries cause very low fracture

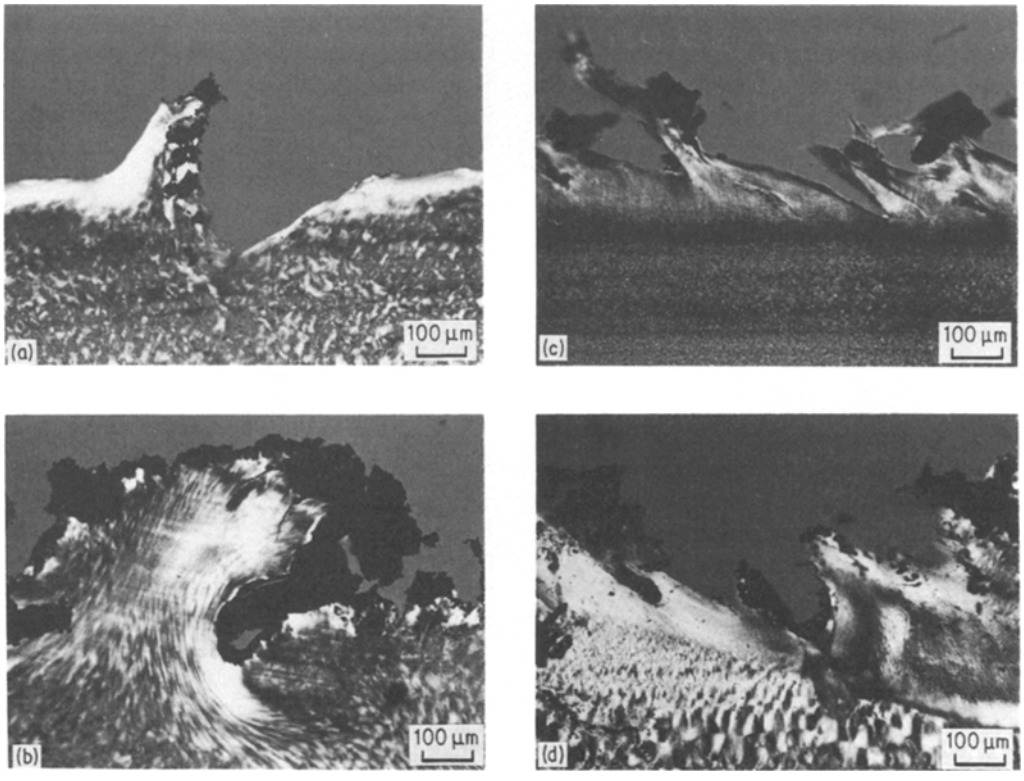

Figure 18 Transmitted light micrographs of thin sections taken from the profiles of eroded samples after 90 min of erosion: (a) PP-A at RT, (b) PP-B at RT, (c) PE at RT, (d) PB-1 at RT.

*"Hard" implies that the balls will suffer no plastic deformation and only negligible elastic deformation during experimentation [4].

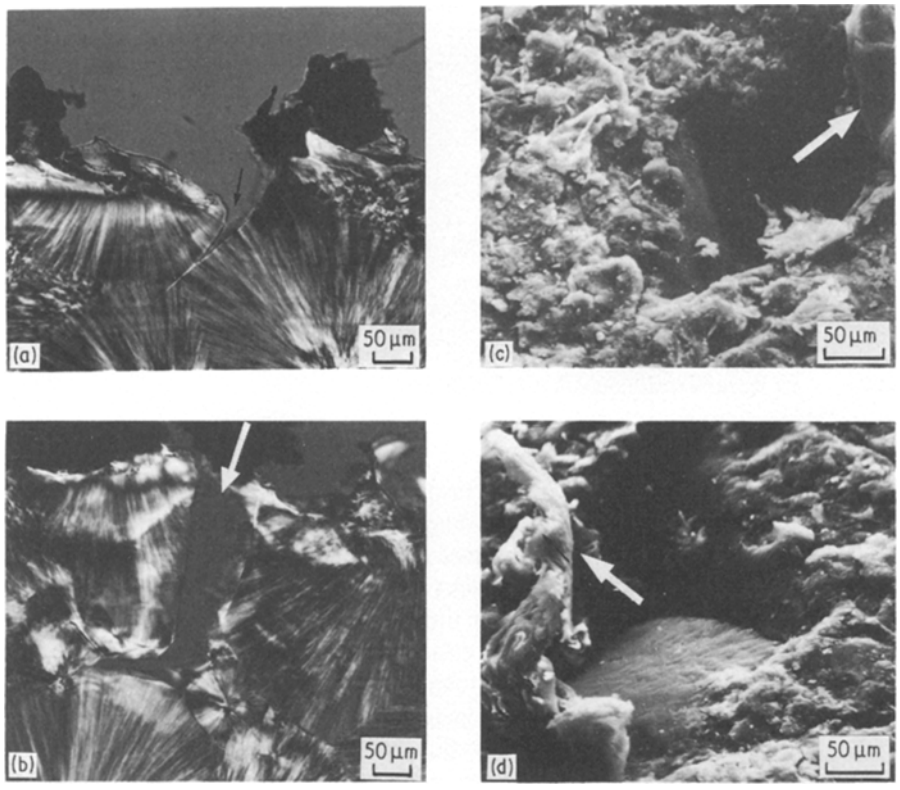

Figure 19 Transmitted light micrographs of PP-A-II surface profiles eroded at (a) RT and (b) −35° C. Both micrographs show preferred surface cracking along the boundaries of the coarse spherulites (arrows). (c, d) Corresponding SEM micrographs of the eroded surfaces showing individual locations where complete spherulites had been broken out of the surface (arrows).

toughness of the material [33]. Fracture under tensile loading is here usually associated with cracking along spherulite boundaries; even under a shear mode of crack opening these sites are preferred for fracture development [34]. Therefore, it is not surpirising that in addition the formation of erosive wear debris is favoured by the presence of these weak planes in the morphology (Fig. 21c).

With respect to the effect of testing temperatures used in this study, no remarkable changes have been observed in the wear mechanisms. A possible explanation for this fact is the possible build-up of heat due to the work done in deforming or cracking the surface in each impact [35]. The eroding surface will rise in temperature if the rate of work done on it exceeds the rate at which heat can flow away through conduction, radiation or forced convection [7]. Under the assumption that the latter effects are almost the same in all of the different polymers tested in this study, the rise in temperature relative to the testing temperature as measured 3 mm away from the sample surface should be the same. The assumption of a temperature rise of about +30° C yields no tremendous difference in the state of ductility for PE, PB-1 (both ductile), or PS (brittle) at both testing temperatures. For the PP variants, however, which undergo a glass transition temperature at $T_g = 0°$ C, the materials should behave in a more brittle manner at the nominal testing temperature of $T = -35°$ C relative to their ductile state at RT testing. The most pronounced effect should be expected for the materials PP-A-II, for which under low-temperature conditions the embrittlement effect and the weak spherulite boundary effect act synergetically in enhancing the mechanisms of material removal, and thus the erosive wear rate.

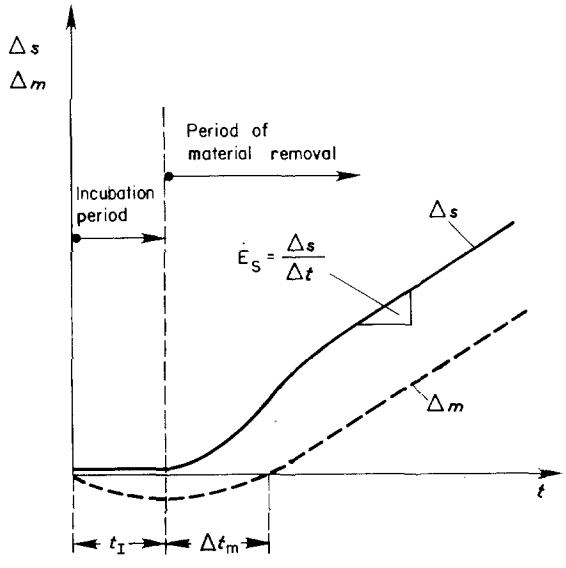

Figure 20 Schematic representation of the height loss (Δs) and the mass loss (Δm) as a function of erosion time (t).

4.2. Correlation of erosive wear rates with other material properties

Referring to the studies on erosion of surfaces by solid particles published by Finnie in 1960 [1], the volume of material, V, removed by erosive grains of mass M and velocity v could be expressed as

$$V = kMv^2 \tag{3a}$$

or, making use of Equations 1 and 2,

$$\dot{E}_s \propto kMv^2 \tag{3b}$$

The term k can be considered as a parameter which takes into account both the characteristic details of external parameters like erodent (material, geometry) and nominal impact angle α, and the mechanical

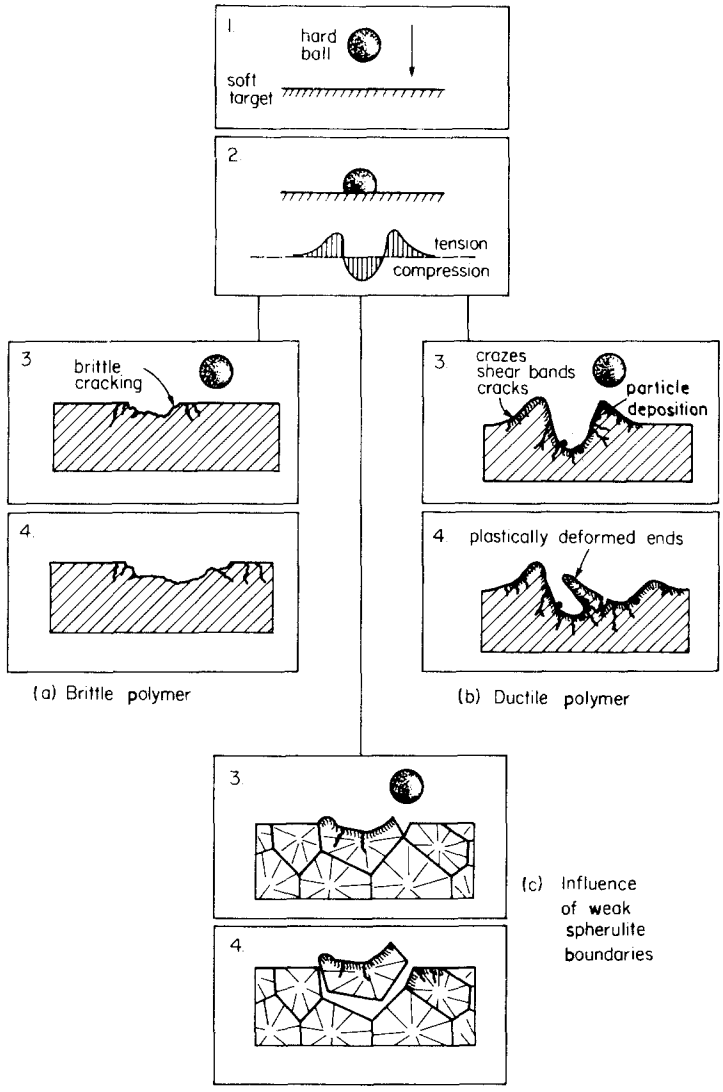

Figure 21 Schematic sketches of sequential surface damage as a result of repeated particle impact on brittle and ductile polymer targets.

property profile of the material tested:

$$k = f(\alpha, \text{erodent, material properties}) \quad (4)$$

If the external conditions are held constant, the erosive wear rate $\dot{E}_s$ should be proportional to that part of parameter k which represents the influence of the material properties (k_e^* = erosive wear factor). For ductile metals it has been found that k_e^* is proportional to the inverse of the plastic flow stress ($\approx$ hardness H) [1, 8, 9]. However, erosion studies on different kinds of polymer and on brittle surface materials have shown clearly that the hardness can cause opposite tendencies as observed for ductile metals [31]. Better correlations for these kinds of material have been found to be based on the fracture energy or a combined term of hardness and fracture toughness [3, 13, 14, 18, 25]. For polymer composites under severe abrasive wear conditions, an expression of the form $(H^{1/2}/G_{Ic})$ has been shown to correlate quite well with the wear rate of these materials [36].

In the present study a modified version of the latter expression, namely H/G_{Ic}, gave a good indication of the erosive wear resistance of the polymers investigated (Tables III and IV, Figs 22a and b). For a better comparison of the results obtained here with those of other investigations on the erosive wear behaviour of polymeric materials, all the data were normalized to the values measured for PE. In fact, doing this for selected polymers tested under different erosion conditions leads in all these cases to the same

TABLE III Normalized erosive wear rate $\dot{E}_s$ and normalized "brittleness index" (H/G_{Ic}) of the polymers tested in this study at room temperature (Fig. 22a)*

No.	Material	$\dot{E}_s$ (μm sec^{-1})	$\dot{E}_s/\dot{E}_{s_{PE}}$	H(MPa)	G_{Ic}(kJ m^{-2})	$(H/G_{Ic})/(H/G_{Ic})_{PE}$
1	PS	15.00	10.34	117	0.9	16.60
2	PE	1.45	1.00	41	5.4	1.00
3	PP-A	1.11	0.77	53	15.0	0.46
4	PP-B	0.23	0.16	31	20.4	0.16
5	PB-1	0.44	0.30	27	13.5	0.26
6	PP-A-I	0.67	0.46	50	21.7	0.30
7	PP-A-II	3.10	2.14	53	1.8	3.90

*v = 57 m sec^{-1}, $\bar{D}$ = 500 μm, $\dot{M}$ = 4.6 g sec^{-1}, α = 90°.

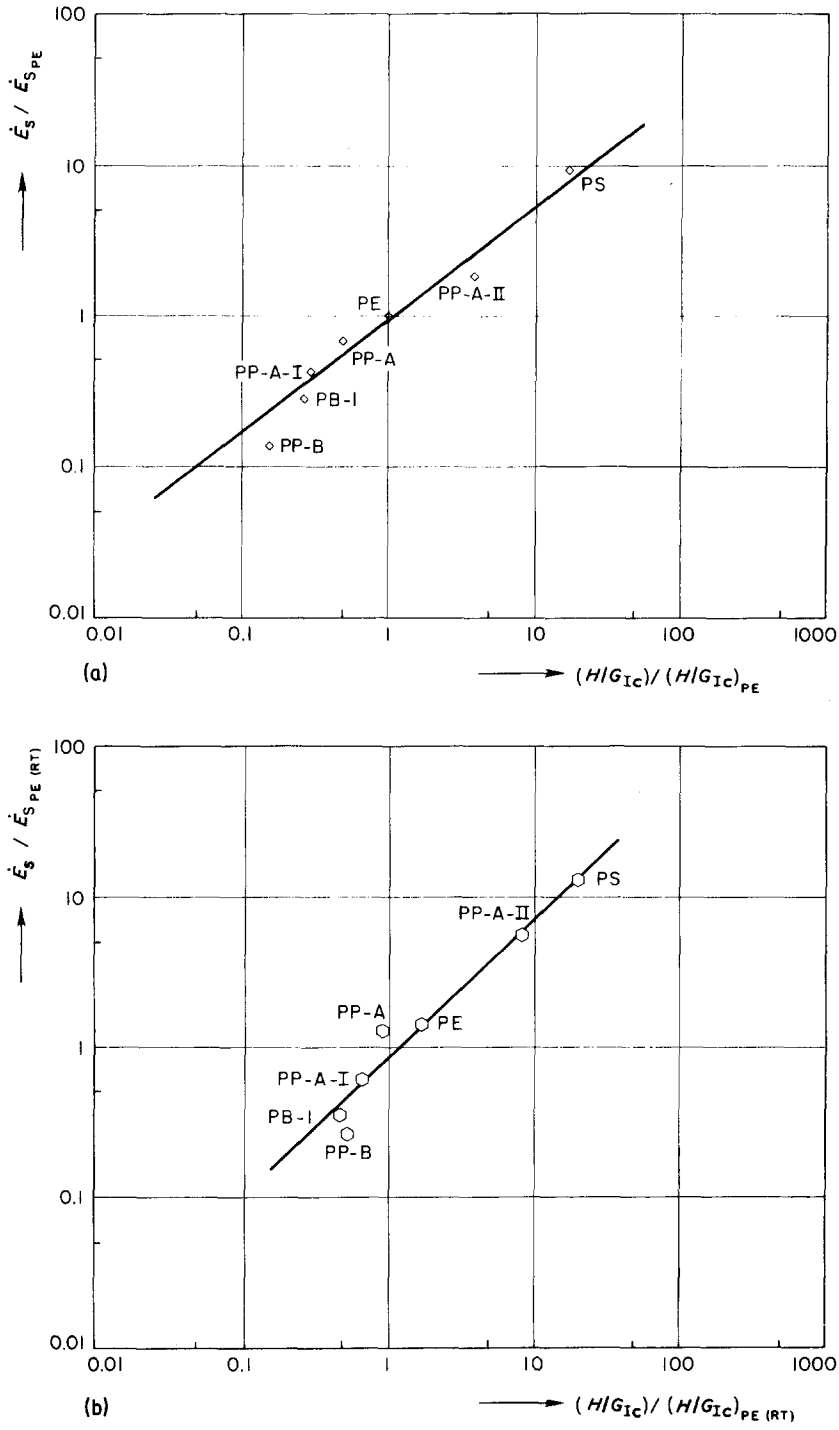

Figure 22 Double logarithmic plot comparing the erosion rate $\dot{E}_s$ with the brittleness index (H/G_{Ic}) of all the materials tested in this study. The data are normalized to the values obtained for PE. Note that the jumps along the line as a result of decreasing testing temperature are highest for the PP variants: (a) T = RT (23° C), (b) $T = -35°$ C, $v = 57\,\mathrm{m\,sec^{-1}}$, $\alpha = 90°$.

trend of $\dot{E}_s$ against H/G_{Ic} (Tables V to VIII; Figs 23 to 26). Only those polymers were selected from the erosive wear papers [12–14, 37] for which corresponding values of H and G_{Ic} (at least of a reasonably assumable size) could be found in other literature sources [26, 38–41]. Fig. 27, which summarizes the results of the different sources, shows that within a scatter of roughly one order of magnitude all the data pairs follow a linear relationship of $\dot{E}_s$ against H/G_{Ic} over about four orders of magnitude when plotted on double-logarithmic scales. Slight differences in slope or relative level of erosive wear rate for a given (H/G_{Ic})

TABLE IV As Table III, but for a testing temperature of −35° C (Fig. 22b)

No.	Material	$\dot{E}_s(\mu\mathrm{m\,sec^{-1}})$	$\dot{E}_s/\dot{E}_{s_{PE/RT}}$	H(MPa)	$G_{Ic}(\mathrm{kJ\,m^{-2}})$*	$(H/G_{Ic})/(H/G_{Ic})_{PE/RT}$
1	PS	17.78	12.26	132	0.9	19.30
2	PE	1.91	1.32	71	5.4	1.73
3	PP-A	1.69	1.17	108	15.0	0.95
4	PP-B	0.33	0.23	82	20.4	0.53
5	PB-1	0.47	0.32	50	13.5	0.49
6	PP-A-I	0.89	0.61	101	21.7	0.61
7	PP-A-II	8.53	5.88	110	1.8	8.04

*Assuming $G_{Ic}(T = -35°\,\mathrm{C}) \approx G_{Ic}(T = 23°\,\mathrm{C})$

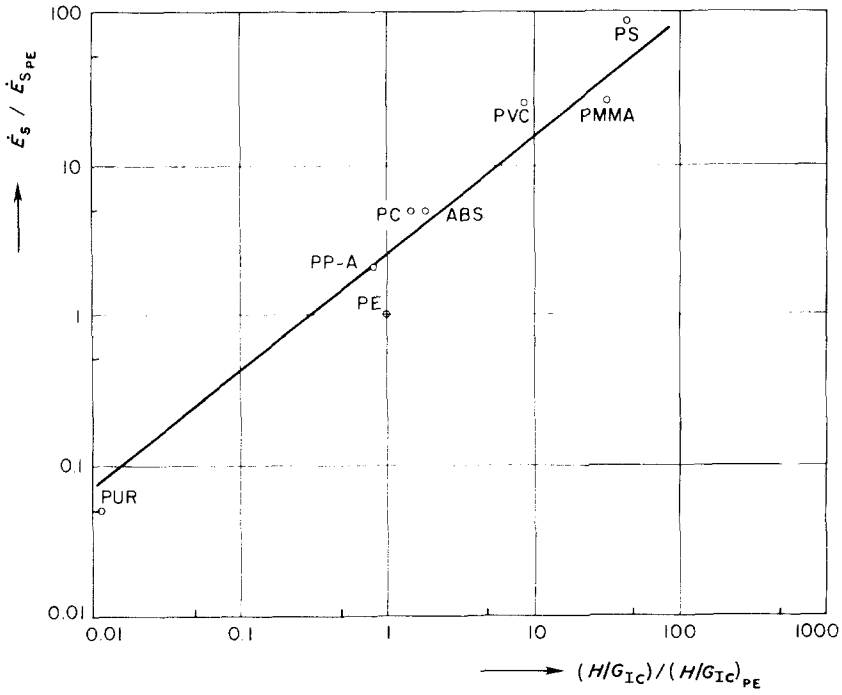

Figure 23 Erosion rate against brittleness index for polymers tested under rain erosion at RT [13]; $v = 410\,\text{m sec}^{-1}$, $\alpha = 90°$.

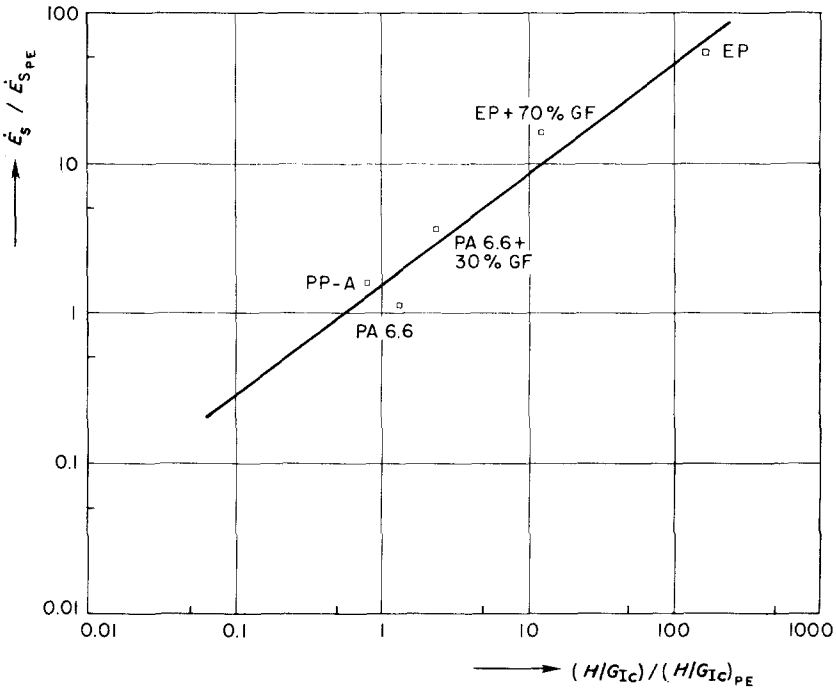

Figure 24 Erosion rate against brittleness index for polymers tested under sand erosion at an angle $\alpha = 90°$ at RT [12]; $v = 243\,\text{m sec}^{-1}$.

TABLE V Erosion rate and brittleness index of polymers tested under rain erosion [13] (Fig. 23)*

No.	Material†	$\dot{E}_s$ (μm sec^{-1})	$\dot{E}_s/\dot{E}_{sPE}$	H(Rockwell R)	G_{Ic}(kJ m^{-2})	$(H/G_{Ic})/(H/G_{Ic})_{PE}$
1	PUR	0.20	0.05	1	13.0	0.01
2	PP-A	8.48	2.01	95	15.0	0.86
3	PC	20.30	4.82	118	10.1	1.58
4	ABS	20.35	4.84	112	8.2	1.84
5	PVC	111.00	26.37	95	1.4	9.16
6	PS	384.50	91.33	110	0.3	45.00
7	PMMA	113.70	27.01	125	0.5	33.06
8	PE(HMW)	4.21	1.00	60	8.1	1.00

*$v = 410\,\text{m sec}^{-1}$, $\bar{D} = 1.2\,\text{mm}$, $\alpha = 90°$.
†PUR = polyurethane, PC = polycarbonate, ABS = acrylonitrile–butadiene–styrene copolymer, PVC = poly(vinyl chloride), PMMA = poly(methyl methacrylate), HMW = high molecular weight.

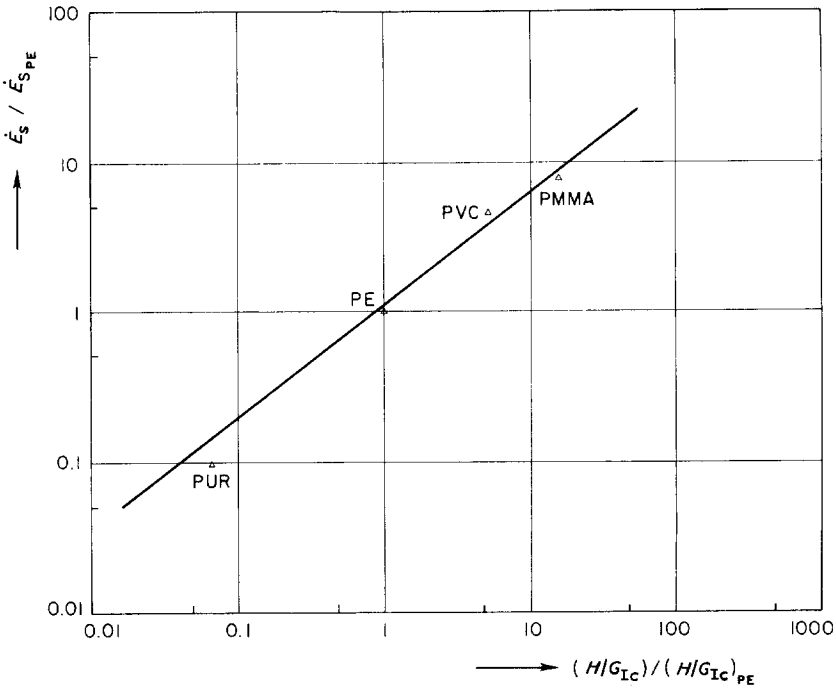

Figure 25 Erosion rate against brittleness index for polymers tested under sand erosion at an angle $\alpha = 45°$ at RT [14]; $v = 77\,\mathrm{m\,sec^{-1}}$.

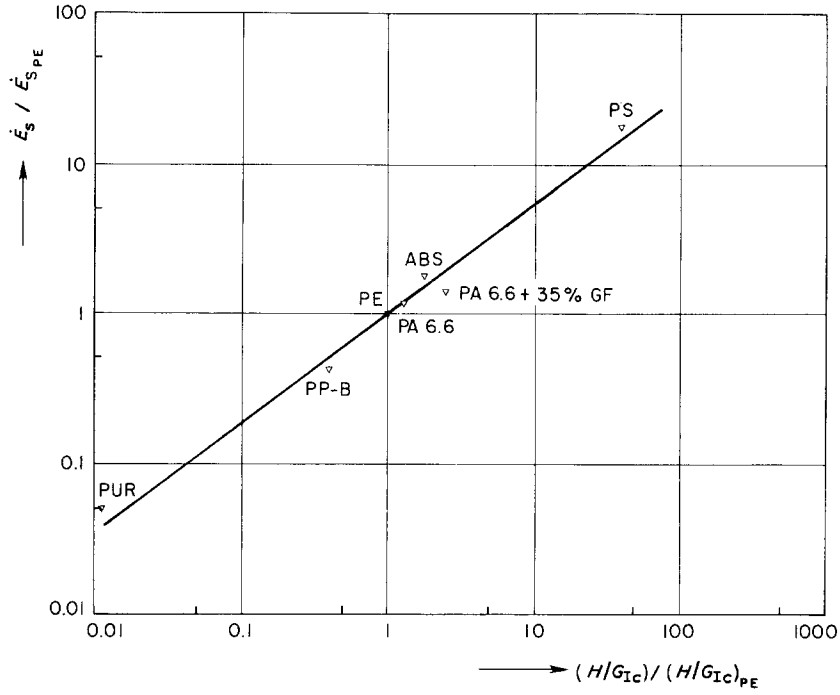

Figure 26 Erosion rate against brittleness index for polymers tested under sand erosion at an angle $\alpha = 45°$ at RT [37]; $v = 40\,\mathrm{m\,sec^{-1}}$.

TABLE VI Erosion rate and brittleness index of polymers tested under quartz sand erosion and an angle α of 90° [12] (Fig. 24)*

No.	Material†	$\dot{E}_s(\mathrm{cm^3\,kg^{-1}})$	$\dot{E}_s/\dot{E}_{s_{PE}}$	H(Rockwell R)	$G_{Ic}(\mathrm{kJ\,m^{-2}})$	$(H/G_{Ic})/(H/G_{Ic})_{PE}$
1	PA 6.6	2.3	1.18	118	12.0	1.33
2	PP-A	3.1	1.57	95	15.0	0.83
3	PA 6.6 + 30% GF	7.0	3.65	121	6.5	2.46
4	EP	100.0	52.18	125	0.1	165.23
5	EP + 70% GF	30.0	15.65	135	1.4	12.75

*$v = 243\,\mathrm{m\,sec^{-1}}$, $\bar{D} = 137\,\mu\mathrm{m}$; ratios (PA 6.6 : PE) taken from Strickle [37].
†PA 6.6 = polyamide, GF = glass fibre, EP = epoxy.

TABLE VII Erosion rate and brittleness index of polymers tested under sand erosion and an angle α of 45° [14] (Fig. 25)*

No.	Material	$\dot{E}_s(\mathrm{mm^3\,h^{-1}})$	$\dot{E}_s/\dot{E}_{s_{PE}}$	H(Shore D)	$G_{Ic}(\mathrm{kJ\,m^{-2}})$	$(H/G_{Ic})/(H/G_{Ic})_{PE}$
1	PUR	–	0.10	18	26.0	0.07
2	PE (HMW)	–	1.00	58	5.4	1.00
3	PVC	–	4.50	78	1.4	5.20
4	PMMA	–	7.68	85	0.5	15.60

*$v = 77\,\mathrm{m\,sec^{-1}}$, $\bar{D} = 400\,\mu\mathrm{m}$, hardness of erodent $\bar{H}_E = 765\,\mathrm{MPa}$.

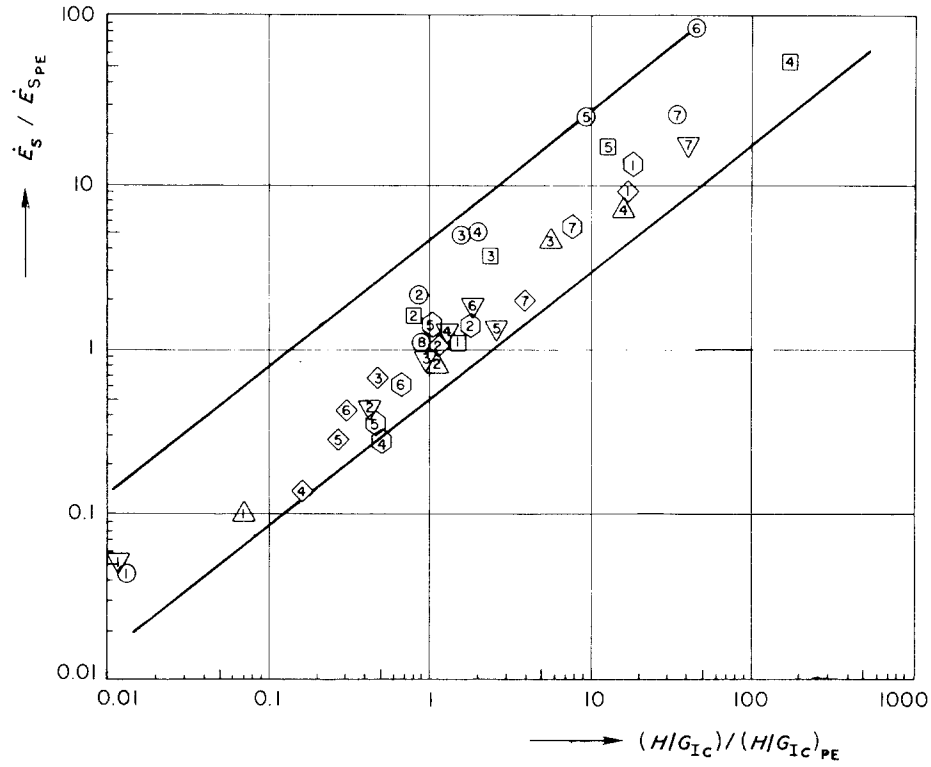

Figure 27 Normalized erosion rate against normalized brittleness index of polymers tested under different erosive wear conditions. Symbols and numbers refer to (◇) Table III, (⬡) Table IV, (○) Table V, (□) Table VI, (△) Table VII, (▽) Table VIII.

value are due to variations in the sensitivity of the materials to differences in the testing conditions (angle α; rain-, steel-, or sand-particles; velocity v, etc.).

5. Conclusions

An air-blast technique has been used to produce steel-ball erosion of different polymeric materials. Testing was carried out at room temperature and at $-35°$ C. The principle conclusions arising from the investigation are as follows:

1. The erosion rate, defined as the reduction in specimen height per testing time, is linear for brittle polymers, such as PS, right from the beginning, whereas the more ductile plastics, such as PE, PP or PB-1, involve an incubation period in which no reduction in height can be measured. Instead, particles become embedded in the surface causing a weight gain. This trend can be, however, changed after further bombardment so that finally a linear rate of erosion is established in this kind of polymer as well.

2. In general, the erosion rate of the ductile polymers is much lower than that of the brittle polymers.

3. A decrease in the specimen temperature leads to an increase in the erosion rate; the latter is most pronounced in those polymers which undergo a ductile–brittle transition by changing the testing temperature.

4. The molecular and morphological structure of semicrystalline polymers has a tremendous effect on the erosion resistance. For example, the less crystalline, highly atactic PP-B exhibited the highest wear resistance. Material PP-A, on the other hand, with a higher crystallinity and lower atactic content, was eroded much faster, especially when the morphology was coarse spherulitic.

5. The erosion rates of the different polymers tested are governed by different material dependences [42]. An increase in hardness, H, for example, may cause an increase in brittle erosion, whereas a higher fracture energy, G_{Ic}, of the material usually leads to an improvement in erosion resistance. It was found that a "brittleness index" term of the form (H/G_{Ic}) can be used as a good indication for the material's erosion resistance (a high brittleness index yields low erosion resistance).

Acknowledgements

Many thanks are due to Dipl.-Ing. H.W. Schröder for

TABLE VIII Erosion rate and brittleness index of polymers tested under sand erosion and an angle α of 45° [37] (Fig. 26)*

No.	Material	$\dot{E}_s$(mm^{3}h^{-1})	$\dot{E}_s/\dot{E}_{s_{PE}}$	H(Rockwell R)	G_{Ic}(kJ m^{-2})	$(H/G_{Ic})/(H/G_{Ic})_{PE}$
1	PUR	8	0.05	1	13.0	0.01
2	PP-B	75	0.44	80	25.0	0.43
3	PE	170	1.00	60	8.1	1.00
4	PA 6.6	200	1.18	118	12.0	1.33
5	PA 6.6 + 35% GF	235	1.38	121	6.5	2.51
6	ABS	290	1.71	112	8.2	1.84
7	PS	2997	17.63	110	0.3	45.00

*v = 40 m sec^{-1}, sand Hard Cast Grade 24.

performing the erosion tests, and to Professor E. Hornbogen, Institute for Materials Science, Ruhr-University Bochum, West-Germany, with whose equipment most of the experiments were carried out. The final form of the paper was prepared during a research stay at the Center for Composite Materials (CCM), University of Delaware, USA. The hospitality and support of the CCM in this respect is gratefully acknowledged. Part of the work was financially supported by the Ministerium für Wissenschaft und Forschung des Landes Nordrhein-Westfalen (IV B 5-FA 19).

References

1. I. FINNIE, *Wear* **3** (1960) 87.
2. G. P. TILLY, *ibid.* **14** (1969) 241.
3. B. LAMY, *Tribol. Int.* **1** (1984) 35.
4. E. B. ITURBE, I. G. GREENFIELD and T. W. CHOU, *Wear* **74** (1981–82) 123.
5. Y. YOKOUCHI, T. W. CHOU and I. G. GREENFIELDS, *Met. Trans.* **14A** (1983) 2415.
6. E. HORNBOGEN, *Fortschr.-Ber. Ver. Deutsch. Ing. Z.* Reihe 5, Nr. 24 (1976).
7. S. M. WALLEY, J. E. FIELD and P. YENNADHIOU, *Wear* **100** (1984) 263.
8. J. GOTZMANN and E. WANDKE, *Schmierungstech.* **14** (1983) 356.
9. K. WELLINGER and H. UETZ, *Wear* **1** (1957–58) 225.
10. J. H. NEILSON and A. GILCHRIST, *ibid.* **11** (1968) 111.
11. H. UETZ and J. FÖHL, *ibid.* **20** (1972) 299.
12. G. P. TILLY and W. SAGE, *ibid.* **16** (1970) 447.
13. G. HOFF and G. LANGBEIN, *Kunststoffe* **1** (1966) 2.
14. H. BRAUER and E. KRIEGEL, *Chemie-Int.-Techn.* **10** (1963) 697.
15. P. V. RAO, S. G. YOUNG and D. H. BUCKLEY, "Solid Spherical Glass Particle Impingement Studies of Plastic Materials", NASA Technical Paper 2161 (1983).
16. R. MELDT, in Proceedings of 5th International Conference on Plastic Pipes, York, 1982 (Plastics and Rubber Institute, London) Paper 29.
17. S. SÖDERBERG, S. HOGMARK, U. ENGMANN and H. SWAHN, *Tribol. Int.* **14** (1981) 333.
18. H. OBERST, *Kunststoffe* **4** (1969) 232.
19. A. I. MAREI and P. V. IZVOZCHIKOV, "Abrasion of Rubber", edited by D. I. James (MacLaren, London, 1967) p. 274.
20. J. K. LANCASTER, *Br. J. Appl. Phys. (J. Phys. D)* **1** (1968) 549.
21. K. FRIEDRICH, *Fortschr.-Ber. Ver. Deutsch. Ing. Z.* Reihe 5, Nr. 82 (1984).
22. S. B. RATNER, I. I. FABEROVA, O. V. RADYUKEVICH and E. G. LUR'E, "Abrasion of Rubber", edited by D. I. James (MacLaren, London, 1967) p. 145.
23. J. K. LANCASTER, *Wear* **14** (1969) 223.
24. B. J. BRISCOE, *Tribol. Int.* **14** (1981) 231.
25. S. M. WIEDERHORN and B. J. HOCKEY, *J. Mater. Sci.* **18** (1983) 766.
26. D. W. VAN KREVELEN and P. J. HOFTYZER, "Properties of Polymers" (Elsevier, Amsterdam, 1976) p. 514.
27. K. FRIEDRICH, in Proceedings of 4th International Conference on Fracture (Fracture 1977), Waterloo, Canada, June 1977, Vol. 3, p. 1119.
28. *Idem, Progr. Colloid Polym. Sci.* **64** (1978) 103.
29. *Idem, ibid.* **66** (1979) 299.
30. P. K. MEHROTRA, G. A. SARGENT and H. CONRAD, *J. Mater. Sci.* **17** (1982) 1042.
31. Y. YOKOUCHI, I. G. GREENFIELD, T. W. CHOU and E. ITURBE, *Met. Trans.* in press.
32. I. G. GREENFIELD and E. ITURBE, *J. Mater. Sci.* in press.
33. E. HORNBORGEN and K. FRIEDRICH, *ibid.* **15** (1980) 2175.
34. K. FRIEDRICH, *Adv. Polym. Sci.* **52/53** 225.
35. D. R. ANDREWS, *J. Phys. D: Appl. Phys.* **14** (1981) 1979.
36. K. FRIEDRICH, in "Friction and Wear of Polymer Composites," edited by K. Friedrich (Elsevier, Amsterdam, 1986) p. 233.
37. E. STRICKLE, private communication (1979).
38. S. S. SCHWARTZ and S. H. GOODMAN, "Plastic Materials and Processes" (Van Nordstrand-Reinhold, New York, 1982) p. 392.
39. H. H. KAUSCH, "Polymer Fracture" (Springer, Berlin, 1978) p. 260.
40. J. G. WILLIAMS, "Fracture Mechanics of Polymers" (Ellis Horwood, Chichester, England, 1984) p. 151.
41. A. J. KINLOCH and R. J. YOUNG; "Fracture Behaviour of Polymers" (Applied Science, London, 1983).
42. G. P. TILLY, *Wear* **14** (1969) 63.

Received 15 October
and accepted 21 November 1985